



**OPEN ACCESS**

# Facile and solvent-free routes for the synthesis of size-controllable $\text{Fe}_3\text{O}_4$ nanoparticles

To cite this article: Thanh Hieu Ngo *et al* 2010 *Adv. Nat. Sci. Nanosci. Nanotechnol.* 1 035001

View the [article online](#) for updates and enhancements.

## You may also like

- [Overview of recent direct wafer bonding advances and applications](#)  
H Moriceau, F Rieutord, F Fournel et al.
- [Modelling the effect of structural QSAR parameters on skin penetration using genetic programming](#)  
K K Chung and D Q Do
- [CdS sensitized ZnO electrodes in photoelectrochemical cells](#)  
Tran Chien Dang, Duy Long Pham, Huu Lam Nguyen et al.

# Facile and solvent-free routes for the synthesis of size-controllable Fe<sub>3</sub>O<sub>4</sub> nanoparticles

Thanh Hieu Ngo<sup>1</sup>, Dai Lam Tran<sup>1</sup>, Hung Manh Do<sup>1</sup>, Vinh Hoang Tran<sup>2</sup>, Van Hong Le<sup>1</sup> and Xuan Phuc Nguyen<sup>1</sup>

<sup>1</sup> Institute of Materials Science, Vietnam Academy of Science and Technology, 18 Hoang Quoc Viet Road, Hanoi, Vietnam

<sup>2</sup> Faculty of Chemical Technology, Hanoi University of Technology, 1 Dai Co Viet Road, Hanoi, Vietnam

E-mail: lamtd@ims.vast.ac.vn

Received 23 July 2010

Accepted for publication 23 September 2010

Published 21 October 2010

Online at [stacks.iop.org/ANSN/1/035001](http://stacks.iop.org/ANSN/1/035001)

## Abstract

Magnetite nanoparticles are one of the most important materials that are widely used in both medically diagnostic and therapeutic research. In this paper, we present some facile and non-toxic synthetic approaches for size-controllable preparations of magnetite nanoparticles, which are appropriate for biomedical applications, namely (i) co-precipitation; (ii) reduction–precipitation and (iii) oxidation–precipitation. Magnetic characterizations of the obtained nanoparticles have been studied and discussed. The oxidation precipitation route was chosen for investigation of the dependence of kinetic driven activation energy and that of coercive force on particle size (and temperature) during the course of the reaction. The structural–magnetic behavior was also correlated. Being solvent and surfactant-free, these methods are advantageous for synthesis and further functionalization towards biomedical applications.

**Keywords:** magnetite nanoparticles, co-precipitation, reduction–precipitation, oxidation–precipitation, activation energy

**Classification numbers:** 4.02, 5.02, 5.08

## 1. Introduction

Magnetite nano-sized particles are of great interest for various biomedical applications, such as the magnetic separation of cells, drug delivery, anticancer therapy, hyperthermia treatment and magnetic resonance imaging, thanks to their interesting physical properties [1–10]. Once each particle is made small, down to 20 nm and less, magnetite nanoparticles can exhibit superparamagnetic behavior, meaning the absence of coercivity [11–13]. Bigger particles, however, are both single-domain and ferromagnetic and hold comparable magnetic coercivity. Currently, the investigation of synthesis and properties is continuing to attract considerable interest from materials scientists. To synthesize monodisperse and uni-sharped particles for biomedical applications, various wet methods have been reported, including co-precipitation, hydrothermal synthesis, microemulsion and

sol–gel. Among the above listed methods, preparative procedures from precipitation is very applicable, thanks to its simplicity, efficiency and ability to control the particle size of magnetites.

A variety of methods have been reported in the literature to synthesize Fe<sub>3</sub>O<sub>4</sub> nanoparticles, such as co-precipitation, thermal decomposition of an alkaline solution of Fe<sup>3+</sup> chelate in the presence of hydrazine, sonochemical decomposition of hydrolyzed Fe-(II) salt, reduction of hematite by CO and organic solution phase decomposition of organometallic precursors [14–16]. Briefly, Fe<sub>3</sub>O<sub>4</sub> nanoparticles can be synthesized by different methods, using different kinds of organic solvents/surfactants. However, the main drawback to these is that with the use of organic solvents/surfactants, these materials remain on the Fe<sub>3</sub>O<sub>4</sub> nanoparticle surface and tend to make it difficult to for them to be encapsulated in a hydrophilic polymer shell for further biomedical applications.

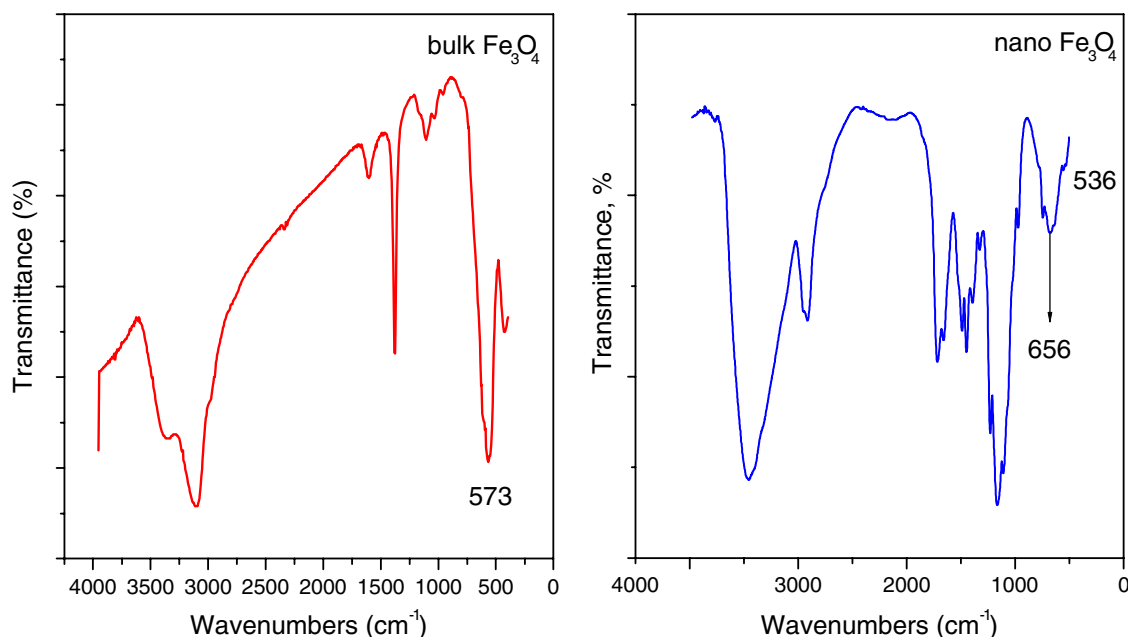


**Figure 1.** IR spectra of bulk and nano  $\text{Fe}_3\text{O}_4$ .

In this study, precipitation based synthetic routes were adjusted for biomedical applications and thoroughly studied in terms of formally kinetic considerations. Superparamagnetic  $\text{Fe}_3\text{O}_4$  nanoparticles were obtained by reduction–precipitation and co-precipitation, whereas ferromagnetic single–domain  $\text{Fe}_3\text{O}_4$  nanoparticles were obtained from oxidation–precipitation. The oxidation–precipitation route was also chosen for further investigation into the dependence of kinetic driven activation energy and that of coercive force on particle size (and temperature) during the course of the reaction.

## 2. Experimental

### 2.1. Materials

All chemicals in this work were of analytical grade and were used without further purification. Ferric chloride hexa-hydrate ( $\text{FeCl}_3 \cdot 6\text{H}_2\text{O}$ ), ferrous chloride tetra-hydrate ( $\text{FeCl}_2 \cdot 4\text{H}_2\text{O}$ ), polyvinyl alcohol (PVA), sodium nitrate ( $\text{NaNO}_3$ ), sodium sulfite ( $\text{Na}_2\text{SO}_3$ ), sodium hydroxide ( $\text{NaOH}$ ) and ammonium hydroxide ( $\text{NH}_4\text{OH}$ , 26% of ammonia) were purchased from Aldrich. Concentrated aqueous ammonium hydroxide was diluted before used.

### 2.2. Synthetic procedures

In this study, three synthetic pathways were proposed to synthesize  $\text{Fe}_3\text{O}_4$  nanoparticles. Firstly, a co-precipitation route was carried out in alkaline media starting from a mixed  $\text{FeSO}_4/\text{FeCl}_3$  solution with a molar ratio of  $\text{Fe(II)}/\text{Fe(III)} = 1 : 2$ , under an inert atmosphere, purged by nitrogen. Diluted aqueous ammonia was added to the mixture. The synthesis was carried out in batches. PVA was used as the surface active agent (0.1%).

Secondly, a reduction–precipitation route starting from a mixed  $\text{FeCl}_3/\text{Na}_2\text{SO}_3$  solution was carried out in air. This

method consists of two steps: partial reduction of ferrous  $\text{Fe}^{3+}$  to ferric  $\text{Fe}^{2+}$  ions and subsequent rapid co-precipitation in an alkaline medium (diluted ammonia) under vigorous stirring for 30 min. The experiments showed that obtained MNPs depend on molar ratio  $R = [\text{Fe}^{3+}]_0/[\text{SO}_3^{2-}]_0$ .

Thirdly, an oxidation–precipitation method was used based on oxidizing iron (II) salts in alkaline solutions by mild oxidants, such as nitrate and air oxygen. In our study, a mixture solution of nitrate sodium and hydroxide sodium was added to a solution of iron (II) chloride. The reaction lasted for 24 h at temperatures of 20, 40, 60 and 80 °C. The nitrate ( $\text{NO}_3^-$ ) concentration was varied in the range of 1.1–3.1  $\text{mg ml}^{-1}$  and was kept constant at 1.5  $\text{mg/ml}^{-1}$  in kinetic study in function of temperature. After the reaction, the black precipitate was purified with distilled water to get magnetite crystallites with the help of a magnet.

### 2.3. Characterization methods

The phase structure of MNPs was studied by x-ray diffraction (SIEMENS D-5000). Infrared (IR) spectra were recorded with a Nicolet 6700 FT-IR Spectrometer, using KBr pellets, in the region of 400–4000  $\text{cm}^{-1}$ , with a resolution of 4  $\text{cm}^{-1}$ . Field Emission Scanning Electron Microscope (FE-SEM) and Transmission Electron Microscope (TEM) images were analyzed by a Hitachi S-4800 and a JEM-1200EX (Voltage: 80 kV, magnification  $\times 100\,000$ ), respectively. The magnetizations versus field were measured with a homemade vibrating sample magnetometer (VSM) and evaluated in terms of saturation magnetization and coercivity.

## 3. Results and discussion

### 3.1. Structural and morphological analyses

First, it was observed that the characteristic absorption band of the Fe–O bond of bulk  $\text{Fe}_3\text{O}_4$  was shifted from 573 to 656  $\text{cm}^{-1}$  (figure 1). Moreover, the shoulder at 537  $\text{cm}^{-1}$

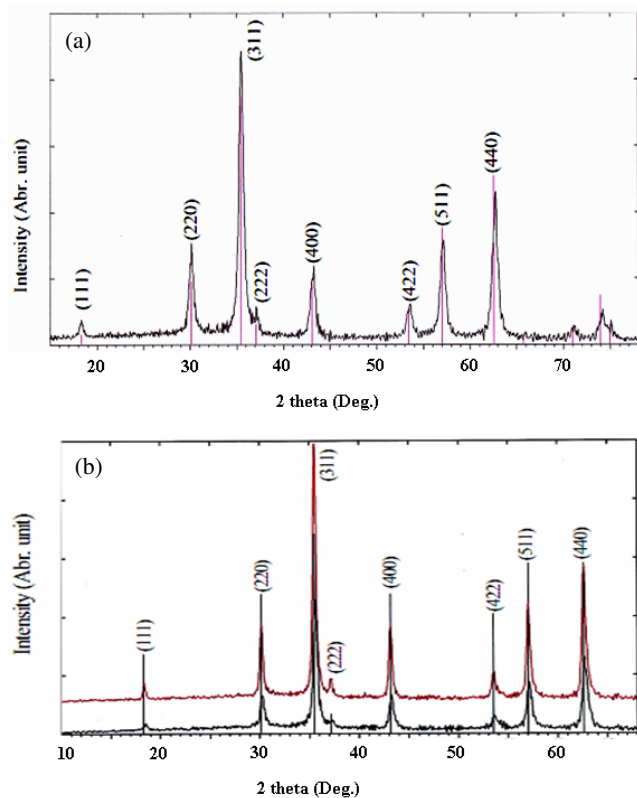


**Figure 2.** XRD patterns of  $\text{Fe}_3\text{O}_4$  nanoparticles obtained by co-precipitation (a) and oxidation-precipitation at different temperatures (b) (black line: at 20 °C, red line: at 40 °C).

near  $656\text{ cm}^{-1}$  appeared. It is well known that an important characteristic of the finite size of nanoparticles is the breaking of a large number of bonds for surface atoms, resulting in the rearrangement of inlocalized electrons on the particle surface. Briefly, the blue-shift of absorption bands of the Fe–O bond of the  $\text{Fe}_3\text{O}_4$  nanoparticles can authenticate the effect of the finite size of nanoparticles [17].

Next, six characteristic peaks for  $\text{Fe}_3\text{O}_4$  corresponding to (220), (311), (400), (422), (511) and (440) were observed in all samples (JCPDS file; PDF No. 65-3107). Quite strong diffraction lines in the patterns observed for the particles synthesized by co-precipitation and oxidation-precipitation (figures 2(a) and 2(b), respectively) indicated that  $\text{Fe}_3\text{O}_4$  particles were well crystallized (peak intensities are 800–1000 cps). It was observed that the increase in temperature favored the degree of their crystallinity.

For the reduction precipitation itself, experiments at different  $R$  values were carried out and XRD patterns of  $\text{Fe}_3\text{O}_4$  nanoparticles were recorded (figure 3). Effectively, XRD patterns demonstrated that pure magnetite can be formed at  $R = 3$ ; i.e. the half value ratio, expected from formally stoichiometric calculation. This is owing to the fact that the reduction reaction is an equilibrium, which can be affected by a number of experimental factors, such as the concentration of HCl,  $\text{FeCl}_3$  and  $\text{Na}_2\text{SO}_3$ , so that  $R = 6$  may not be the ideal initial ratio.

TEM images and particle size distribution of different types of  $\text{Fe}_3\text{O}_4$  prepared by the above listed procedures are presented in figure 4. TEM estimated  $d$  values are

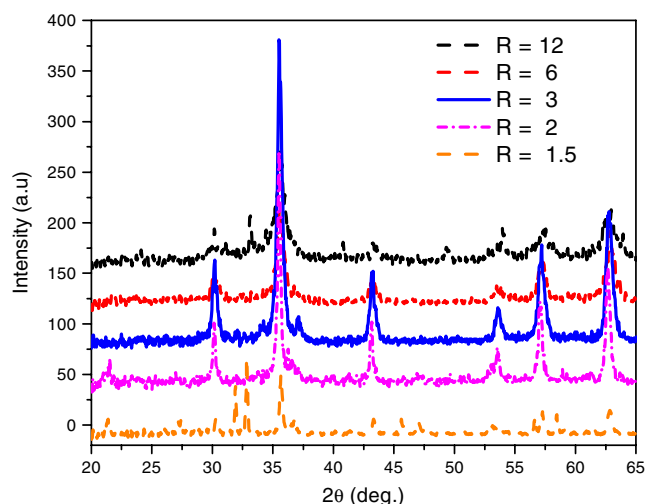


**Figure 3.** XRD patterns of  $\text{Fe}_3\text{O}_4$  nanoparticles by reduction precipitation at different ratios of  $R$  ( $R = [\text{Fe}^{3+}]_0/[\text{SO}_3^{2-}]_0$ ).

summarized in table 1. As shown in this figure,  $\text{Fe}_3\text{O}_4$  nanoparticles are either roughly spherical or cubic in the case of the oxidation-precipitation particles. Smaller particle sizes (10–30 nm) were obtained from co-precipitation and reduction precipitation, while bigger particles (30–70 nm) were formed from oxidation-precipitation. The synthetic route-particle size-dependent phenomenon will be explained from a kinetic point of view in the subsection below.

### 3.2. Kinetic study of $\text{Fe}_3\text{O}_4$ nanoparticle formation

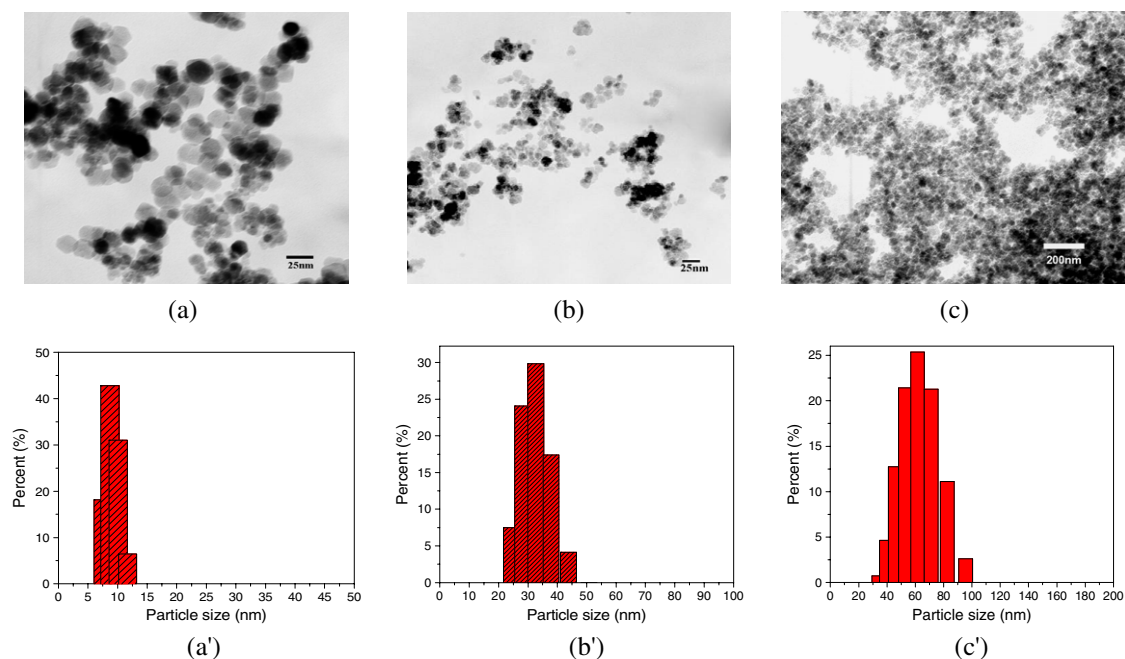
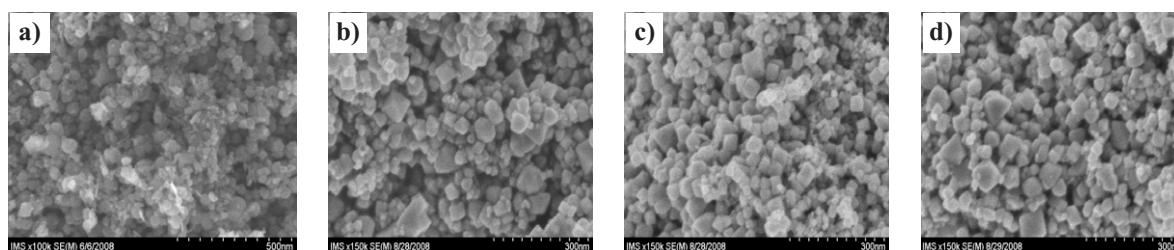
Effectively, route-particle size dependence can be explained in terms of the reaction rate. The formation of larger particles occurs when the number of nuclei decreases and the particle growth increases at the expense of the smaller ones. In the three aforementioned methods, under the same reaction temperature, the reaction rate decreases in the following order: co-precipitation > reduction precipitation > oxidation-precipitation. The co-precipitation reaction proceeds at a very high rate since  $\text{Fe}_3\text{O}_4$ , as a black precipitate is simultaneously formed after the addition of alkaline solution to the mixture of ferrous and ferric salts, as can be experimentally observed, leading to a considerable number of nuclei. As for reduction precipitation and oxidation-precipitation, the reactions are slower with multiple intermediate steps, including complexation and gelation, respectively [18].

Further, to get closer insights into  $\text{Fe}_3\text{O}_4$  formation and to have a better understanding of the conjunct influence of  $T$  on  $d$ , the oxidation-precipitation method was chosen for an investigation of the temperature-particle size ( $T$ – $d$ ) relationship.

Figure 5 presents FE-SEM images of  $\text{Fe}_3\text{O}_4$  nanoparticles prepared by oxidation-precipitation at different temperatures (20–80 °C). It is evident that the sizes of the obtained samples were all above 30 nm, and much larger than those of the samples prepared by co-precipitation or reduction-precipitation. Moreover, the average size decreases as temperature increases. At first sight, this result seemed to be questionable, and attempts were made to elucidate the complicated correlation of the reaction temperature and

**Table 1.** Fe<sub>3</sub>O<sub>4</sub> nanoparticles synthesized by oxidation–precipitation (O1–O4 samples): TEM estimated average particle size, saturation magnetization  $M_s$  and coercive field  $H_c$ .

Sample	Reaction temperature (°C)	Average particle size (nm)	$M_s$ (at 11 kOe) (emu/g <sup>-1</sup> )	$H_c$ (Oe)
O1	20	60 ± 5	62	107
O2	40	51 ± 5	77.6	106
O3	60	43 ± 4	79.5	88
O4	80	35 ± 4	77	82

**Figure 4.** TEM images and histograms of particle size distribution of Fe<sub>3</sub>O<sub>4</sub> nanoparticles synthesized by 3 synthetic routes: co-precipitation (a and a'), reduction (b and b') and oxidation (c and c').**Figure 5.** FE-SEM images of Fe<sub>3</sub>O<sub>4</sub> nanoparticles synthesized by oxidation at different temperatures: (a) 20 °C, (b) 40 °C, (c) 60 °C, (d) 80 °C.

particle size and its influence on the magnetic coercivity. Effectively, according to either thermodynamic or kinetic considerations, temperature is an important factor that can work on the size, dispersibility and crystallinity of Fe<sub>3</sub>O<sub>4</sub>. On the one hand, from the classically thermodynamic point of view, the driving force for particle formation is the change in Gibbs free energy  $\Delta G$ , for transfer from supersaturated solution to equilibrium. The crystallization process is described by the function of the nucleation rate (formation of new crystals) and crystal growth (increase in crystal dimension or agglomeration). Therefore, the particle sizes and their distribution are dictated by the rate ratio of these two processes: fast nucleation tends to produce smaller particles, while predominated growth will induce agglomerates. Normally, with an increase in reaction temperature, the process of ripening would be accelerated, i.e. smaller

nanoparticles would more easily tend to aggregate into bigger particles, leading to the widening of the size distribution. Thus, in our study, under given experimental conditions, the growth process was not strong enough, so nucleation had a predominant effect on the final particle size. Otherwise, the number of nuclei would increase more significantly than nucleus growth itself with increasing temperature, and therefore the obtained Fe<sub>3</sub>O<sub>4</sub> nanoparticles would decrease in size slightly within the studied temperature range. This decreasing tendency of particle size with temperature was also reported by Nishio *et al* [19].

On the other hand, from a kinetic point of view, although not sufficiently rigorous, it could be logically assumed that  $d$  would be approximately proportional to the reaction rate  $v$  and the reaction time  $t$  and the  $T$ – $d$  relationship, derived from the well-known Arrhenius equation, which can be rewritten

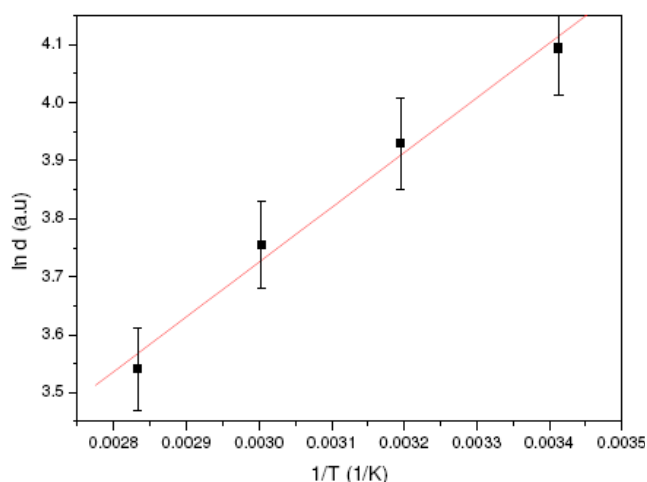


Figure 6. Plot of  $\ln d$  versus  $1/T$ .

in the following form:

$$\ln \frac{v_{T_2}}{v_{T_1}} = \ln \frac{k_{T_2}}{k_{T_1}} = \ln \frac{d_{T_2}}{d_{T_1}} = -\frac{E_a}{R} \left( \frac{1}{T_2} - \frac{1}{T_1} \right), \quad (1)$$

where  $v$  and  $k$  are the rate and rate constants at a given temperature, respectively,  $d$  is the particle size,  $E_a$  is the activation energy and  $R$  is the gas constant. Using this equation, some kinetic parameters (especially activation energy  $E_a$ ) could be qualitatively assessed. In fact, in the  $\text{Fe}_3\text{O}_4$  formation process, a two-step reaction would proceed, simultaneously in the forward and backward directions, as follows:



The activation process (3) is much slower than process (2) and is therefore the rate-determining stage. The plot of  $\ln k$  ( $\ln d$ ) versus  $1/T$  shows a linear behavior in the studied temperature range (40–80 °C), indicating that the assumption made for equation (1) appears to be reasonably valid based on the limited set of available experimental data (figure 6).

The value of  $E_a$  is physically meaningful and worth discussing. First, according to the Arrhenius equation, if  $E_a$  is close to zero, the reaction is diffusion controlled and the rate constant is equal to the pre-exponential factor. Hence, the pre-exponential factor for a given reaction is identical to the diffusion controlled rate constant. Further,  $E_a$  was found to be associated with the surface energy of the small nuclei. Once the nuclei grow to a stage when an additional atom can be accommodated in the bulk of the particle, the surface energy per mole of atoms will start to decrease, indicating the end of the nucleation stage. The activation energy can therefore be approximated by the surface energy per mole of atoms of an ensemble of ‘critical’ nuclei. So, particle size should affect the activation energy of the process and  $\text{Fe}_3\text{O}_4$  with different sizes should possess different values of  $E_a$ .

By repeating the calculations at various particle sizes (obtained at various  $T$ , respectively), it is possible to determine approximately  $E_a$  of the process whose values fall within the range of 6.2–10.1 kJ mol<sup>-1</sup>, depending on the value selected set of  $d$  (and  $T$ , respectively): the bigger  $d$

is (lower  $T$ ), the lower  $E_a$  will be (table 2). It should be noted that the obtained values are somewhat different from the reported data for  $\text{Fe}_3\text{O}_4$  bulk material (5.6 kJ mol<sup>-1</sup>) [20]. From the aforementioned consideration, it can be inferred that the discrepancy in  $E_a$  should be related to the particle size effect. Certain expectations regarding the dependence of  $E_a$  on the particle size effect can be extracted from the fact that larger particles contain more electrons than smaller ones. Hence, the barrier for the removal of electrons (per m<sup>2</sup>) from the particle should decrease with increasing electron content since the number of surface sites increases with  $r^2$  while the number of electrons increases with  $r^3$ . A simple approach would then be to describe the activation energy based on the Boltzmann distribution. Without a detailed mathematical description of this distribution here, it can be concluded that the deviation in  $E_a$  for a nanosized particle compared to the bulk material should be proportional to the logarithm of the particle radius  $r$ . In summary, this result reconfirmed that many physicochemical properties (including  $E_a$ ) of nanosized particles are known to differ significantly from those of bulk materials.

### 3.3. Magnetic properties

Figure 7(a) presents the magnetization curves of  $\text{Fe}_3\text{O}_4$  nanoparticles prepared by different preparative methods. The superparamagnetic and nanosized behavior of  $\text{Fe}_3\text{O}_4$  nanoparticles, observed in co-precipitation and reduction–precipitation, was documented by the hysteresis loop with almost immeasurable coercivity (a few Oe) at room temperature (300 K). Unlike those nanoparticles obtained by co-precipitation and reduction–precipitation, the nanoparticles synthesized by oxidation have shown a larger coercivity (80–100 Oe). Also, the non-zero coercivity in the later samples has evidenced a soft magnetic character, or so-called single-domain ferromagnetic nature of nanoparticles.

According to figure 7(a), the saturation magnetization of  $\text{Fe}_3\text{O}_4$  particles is in the range of 60–80 emu g<sup>-1</sup> and is lower than that of bulk  $\text{Fe}_3\text{O}_4$  (about 90 emu g<sup>-1</sup>). This discrepancy in  $M_s$  can result from the difference in particle size obtained by various synthetic routes, as it has been reported in the literature that saturation magnetization of  $\text{Fe}_3\text{O}_4$  nanoparticles decreases with decreasing particle size. Further, hysteresis loops of  $\text{Fe}_3\text{O}_4$  nanoparticles prepared by oxidation–precipitation at different temperatures (20–80 °C) and at a fixed concentration of  $\text{NO}_3^-$  were shown in figure 7(b). It was found that  $\text{Fe}_3\text{O}_4$  nanoparticles exhibited rather high saturation magnetization (60–80 emu g<sup>-1</sup>) and this value almost does not change as the temperature increases from 40 to 80 °C. The clear decrease in coercivity as the reaction temperature increases was also observed (table 2). Moreover, it was noted that the increase in  $\text{NO}_3^-$  concentration has resulted in larger particles with a wider size distribution (figure not shown), whereas it has a slight effect on saturation magnetizations and coercive forces ( $M_s = 60$ –70 emu g<sup>-1</sup>,  $H_c = 54$ –100 Oe; figure 7(c)).

Next, the dependence of the coercivity force  $H_c$  on particle size has already been studied in the literature [21]. When the particle size is less than single-domain size  $r_c$

**Table 2.** Calculated activation energy  $E_a$  at differently available temperature set.

Temperature set ( $T_1; T_2$ )	(20;40)	(20;60)	(40;60)	(20;80)	(40;80)	(60;80)
Activation energy ( $E_a$ , $\text{kJ mol}^{-1}$ )	6.2	6.8	7.4	7.7	8.6	10.1

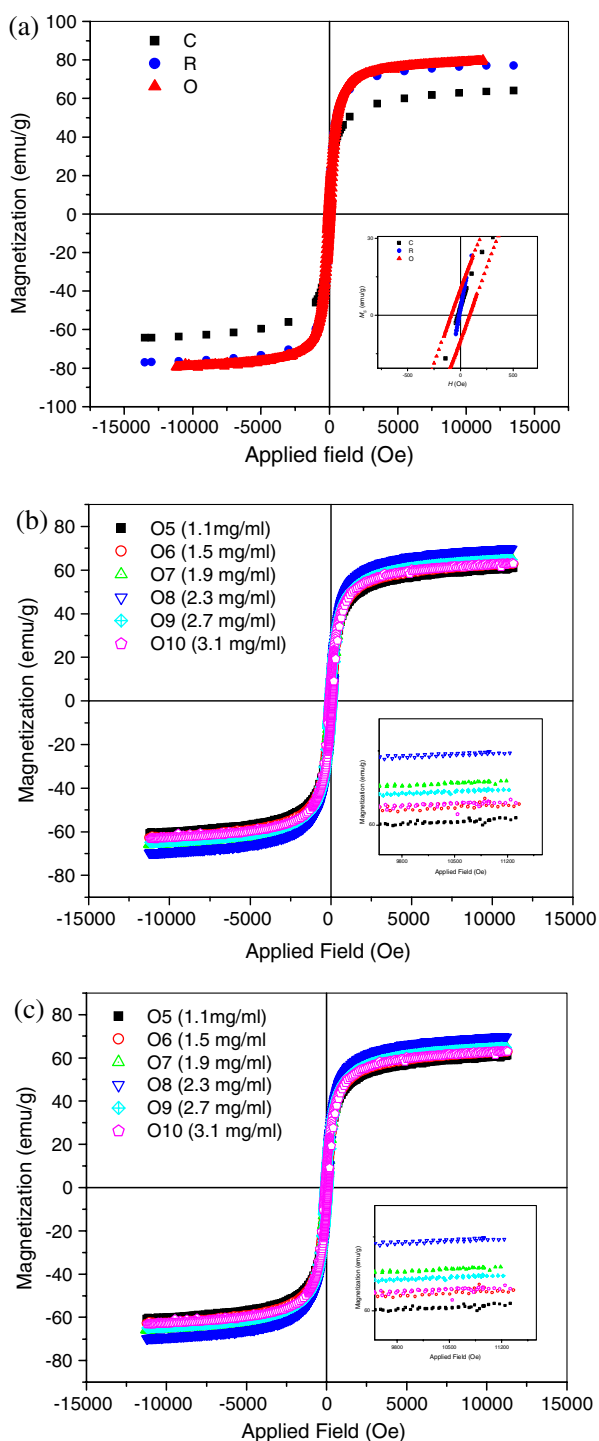


**Figure 7.** (a) Hysteresis loops of  $\text{Fe}_3\text{O}_4$  nanoparticles, synthesized by three synthetic routes: C: co-precipitation; O: oxidation-precipitation; R: reduction precipitation (the inset shows the zoomed hysteretic loop from  $-200$  to  $200$  Oe). (b) Hysteresis loops of  $\text{Fe}_3\text{O}_4$  nanoparticles, synthesized by oxidation-precipitation at different temperatures (O1–O4 samples; the inset shows the zoomed hysteretic loop from  $-200$  to  $200$  Oe). (c) Hysteresis loops of  $\text{Fe}_3\text{O}_4$  nanoparticles, synthesized by oxidation-precipitation at different  $\text{NO}_3^-$  concentrations (O5–O10 samples; the inset shows the zoomed hysteretic loop from  $-9$  to  $11.3$  kOe).

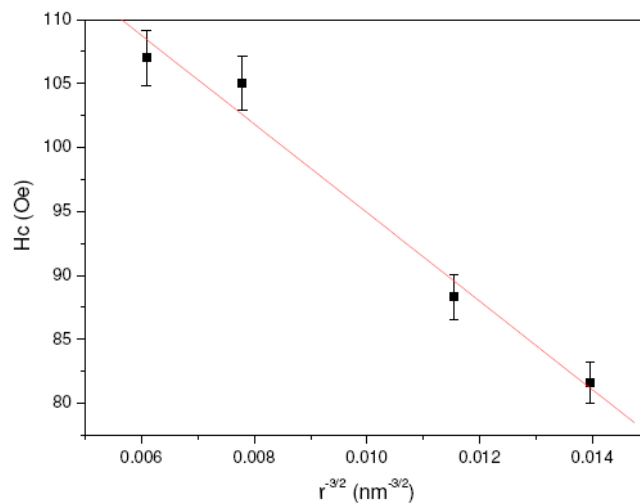


**Figure 8.** Experimental and fitted dependence of coercivity on particle size

and the particles are not interacting with each other, the dependence can be described as  $H_c = a - b/r^{3/2}$ , where  $H_c$  is the coercivity force,  $a$  and  $b$  are constants and  $r$  is the particle radius. As can be seen from figure 8, it is reasonable to confirm that experimental and calculated values of  $H_c$  in the function of particle radius  $r$  are very consistent. Constants  $a$  and  $b$  can be calculated as  $136.1$  Oe and  $3986.9$  Oe  $\text{nm}^{3/2}$ , respectively. The maximum value of coercivity of the single-domain  $\text{Fe}_3\text{O}_4$  particles, as can be referred to the value of  $a$ , is therefore not over  $136.1$  Oe. By extrapolating the plot to  $H_c \approx 0$ , the particle radius  $r$  could be obtained approximately as  $9.5$  nm, very close to that of superparamagnetic particles, which has been experimentally proven and reported in the literature [1].

#### 4. Conclusions

In conclusion, facile routes to prepare size-controllable  $\text{F}_3\text{O}_4$  powders have been presented. Some attempts have been made to establish structural-magnetic property dependence. Being economical, and solvent- and surfactant-free, the present synthetic approaches have some advantages compared to those previously reported in the literature, which makes them suitable for scaling up to mass production and for addressing biomedical applications.

#### Acknowledgments

The authors are grateful for the financial support for this work from a VAST key research project granted to IMS (2009–2010) and a Korean–Vietnamese joint research project (2010–2011, code: 59/2615/2010/HĐ-NĐT). The authors would like to acknowledge their indebtedness to Professor Acad. Nguyen Van Hieu is thanked for his constant encouragement and support of their work.

## References

- [1] Cornell R M and Schwertmann U 1996 *The Iron Oxides: Structure, Properties, Reactions, Occurrence and Uses* (New York: VCH)
- [2] Pankhurst Q A, Connolly J, Jones S K and Dobson J 2003 *J. Phys. D: Appl. Phys.* **36** R167
- [3] Mornet S, Vasseur S, Grasset F and Duguet E 2004 *J. Mater. Chem.* **14** 2161
- [4] O'Grady K 2009 *J. Phys. D: Appl. Phys.* **42** 220301
- [5] Gupta A K and Gupta M 2005 *Biomaterials* **26** 3995
- [6] Berry C C and Curtis A S G 2003 *J. Phys. D: Appl. Phys.* **36** R198
- [7] Salata O V 2004 *J. Nanobiotechnol.* **2** 3
- [8] Ito A, Shinkai M, Honda H and Kobayashi T 2005 *J. Bioeng.* **100** 1
- [9] Tartaj P, Morales M P, González-Carreño T, Veintemillas-Verdaguer S and Serna C J 2005 *J. Magn. Magn. Mater.* **291** 28
- [10] Pankhurst Q A, Thanh N K T, Jones S K and Dobson J 2009 *J. Phys. D: Appl. Phys.* **42** 224001
- [11] Qu S C, Yang H B, Ren D W, Kan S H, Zou G T, Li D M and Li M H 1999 *J. Colloid Interface Sci.* **215** 190
- [12] Lee Y J, Lee J W, Bae C J, Park J G, Noh H J, Park J H and Hyeon T G 2005 *Adv. Funct. Mater.* **15** 503
- [13] Vayssieres L 2005 *Int. J. Nanotechnol.* **2** 411
- [14] Capek I 2006 *Nanocomposite Structures and Dispersions: Science and Nanotechnology—Fundamental Principles and Colloidal Particles Studies in Interface Science* vol 23 ed D Mobius and R Miller (Amsterdam: Elsevier)
- [15] Ettabirou M, Dupré B and Gleitzer C 1986 *React. Solids* **1** 329
- [16] Wostek-Wojciechowska D, Jeszka J K, Amiens C, Chaudret B and Lecante P 2005 *J. Colloid Interface Sci.* **287** 107
- [17] Ma M, Zhang Y, Yu W, Shen H Y, Zhang H Q and Gu N 2003 *Colloid Surface A* **212** 219
- [18] Sugimoto T and Matijevic E 1980 *J. Colloid Interface Sci.* **74** 227
- [19] Nishio K, Ikeda M, Gokon N, Tsubouchi S, Narimatsu H, Mochizuki Y, Sakamoto S, Sandhu A, Abe M and Handa H 2007 *J. Magn. Magn. Mater.* **310** 2408
- [20] Kazlowaski A, Rasmussen R J, Sabol J E, Metacalf P and Honig J M 1993 *Phys. Rev. B* **48** 2057
- [21] O'Handley R C 2000 *Modern Magnetic Materials—Principles and Applications* (New York: Wiley)